JOURNAL OF THE ROYAL SOCIETY Interface

rsif.royalsocietypublishing.org

Research

Cite this article: Craddock TJA, Friesen D, Mane J, Hameroff S, Tuszynski JA. 2014 The feasibility of coherent energy transfer in microtubules. *J. R. Soc. Interface* **11**: 20140677. http://dx.doi.org/10.1098/rsif.2014.0677

Received: 26 June 2014
Accepted: 22 August 2014

Subject Areas:
biophysics, chemical physics, computational biology

Keywords:
energy transfer, quantum biology, optical spectra, microtubule, structure-based simulation

Author for correspondence:
Travis John Adrian Craddock
e-mail: tcraddock@nova.edu

The feasibility of coherent energy transfer in microtubules

Travis John Adrian Craddock[1,2], Douglas Friesen[3], Jonathan Mane[3], Stuart Hameroff[4] and Jack A. Tuszynski[3,5]

[1]Center for Psychological Studies, Graduate School of Computer and Information Sciences, and College of Osteopathic Medicine, Nova Southeastern University, Ft Lauderdale, FL 33328, USA
[2]Institute for Neuro-Immune Medicine, Nova Southeastern University, Ft Lauderdale, FL 33328, USA
[3]Department of Oncology, University of Alberta, Cross Cancer Institute, Edmonton, Alberta, Canada T6G 1Z2
[4]Departments of Anesthesiology and Psychology, Center for Consciousness Studies, The University of Arizona Health Sciences Center, Tucson, AZ 210202, USA
[5]Department of Physics, University of Alberta, Edmonton, Alberta, Canada T6G 2E1

It was once purported that biological systems were far too 'warm and wet' to support quantum phenomena mainly owing to thermal effects disrupting quantum coherence. However, recent experimental results and theoretical analyses have shown that thermal energy may assist, rather than disrupt, quantum coherent transport, especially in the 'dry' hydrophobic interiors of biomolecules. Specifically, evidence has been accumulating for the necessary involvement of quantum coherent energy transfer between uniquely arranged chromophores in light harvesting photosynthetic complexes. The 'tubulin' subunit proteins, which comprise microtubules, also possess a distinct architecture of chromophores, namely aromatic amino acids, including tryptophan. The geometry and dipolar properties of these aromatics are similar to those found in photosynthetic units indicating that tubulin may support coherent energy transfer. Tubulin aggregated into microtubule geometric lattices may support such energy transfer, which could be important for biological signalling and communication essential to living processes. Here, we perform a computational investigation of energy transfer between chromophoric amino acids in tubulin via dipole excitations coupled to the surrounding thermal environment. We present the spatial structure and energetic properties of the tryptophan residues in the microtubule constituent protein tubulin. Plausibility arguments for the conditions favouring a quantum mechanism of signal propagation along a microtubule are provided. Overall, we find that coherent energy transfer in tubulin and microtubules is biologically feasible.

1. Introduction

Since Schrodinger asked 'what is life?' [1], a possible link between the 'weird' world of quantum phenomena and biology has been hypothesized. It has often been argued that living systems are too 'warm and wet' to support quantum effects; however, recent research suggests this is not necessarily always the case. From quantum coherent transport in photosynthesis and magnetoreception in birds to quantum olfaction [2] and single-photon effects in vision [3], the field of quantum biology is leaping into the mainstream. This leads us to inquire, where else might the effects of quantum biology be found?

Without a doubt, the standard bearer for the emergence of quantum biology has been the long-lived electronic quantum coherence found in the light harvesting antennae used in photosynthesis. In 2007, Engel *et al*. [4] directly observed quantum oscillations caused by electronic coherence at 77 K in the Fenna–Matthews–Olsen (FMO) photosynthetic light-harvesting complex (LHC), a temperature pushing the 'warm' limit for quantum processes, catapulting this field into the spotlight [4]. This limit was further pushed to 277 K, nearing physiological temperature, and effectively ruling out the 'warm and wet' limit for quantum phenomena in biology [5]. Furthermore, these coherent

Royal Society Publishing

effects do not seem to be restricted to the FMO complex alone, and have been shown for LHCs in plants (LHCII) [6–8], bacteria (LH2) [9,10] and phycobiliproteins [11,12].

The theoretical basis of this coherent energy transfer is the photo-induced interaction of transition dipoles in chlorophyll molecules. The unique chromophoric nature of chlorophyll and the elegant geometrical arrangement of these pigments in the LHCs of plants and bacteria allow for photon energy to be efficiently captured and funnelled from the environment to reaction centres. This biological light harvesting critically depends on the quantum mechanism through which photon-induced excitations hop between chromophores [13]. An initially excited donor chromophore can convey its electronic energy to an acceptor chromophore via electrodynamic coupling of their transition electric dipole moments owing to the close correspondence, or 'resonance', between their energy levels. This resonance energy transfer (RET), which was originally pioneered by Förster [14] and is more specifically termed FRET, remains the dominant theory applied in electronic energy transport [15,16]. However, this process is not unique to photosynthesis. J-aggregates (aka Scheibe aggregates), collections of dye molecules, are an artificial form of LHC capable of capturing and manipulating photon energy [17,18]. At the root, this phenomenon is attributable to the optimal packing of chromophores with a significant transition dipole.

Interestingly, tubulin, the microtubule constituent protein, possesses a network of chromophoric tryptophan (Trp) amino acids (figure 1). The fluorescence quantum yield for pure Trp is 0.14, and the experimentally observed yield for wild-type tubulin is 0.06 at room temperature [19]. These are comparable to the room temperature fluorescence quantum yields of bacteriochlorophyll of 0.18, and the yield for LH1 of 0.08 and LH2 of 0.10 [20], respectively. The 'red edge effect' has also been observed in tubulin [21] indicating Trp to Trp energy transfer [22]. Thus, these may serve as potential conduction pathways in tubulin and microtubules [23]. Could these aromatic chromophores support coherent quantum effects within tubulin? As persistent electronic coherences may be a general property of any system of compact nearly static chromophores coupled to the environment [24], we investigate the biological feasibility of coherent energy transfer in the tubulin dimer. Via a combination of homology modelling, molecular dynamics (MD) simulations, quantum chemistry and optical biophysics, we apply structure-based simulations similar to current studies of the FMO complex [25,26], and larger LHCs [27] to probe potential energy transfer mechanisms in tubulin, and by extension microtubules.

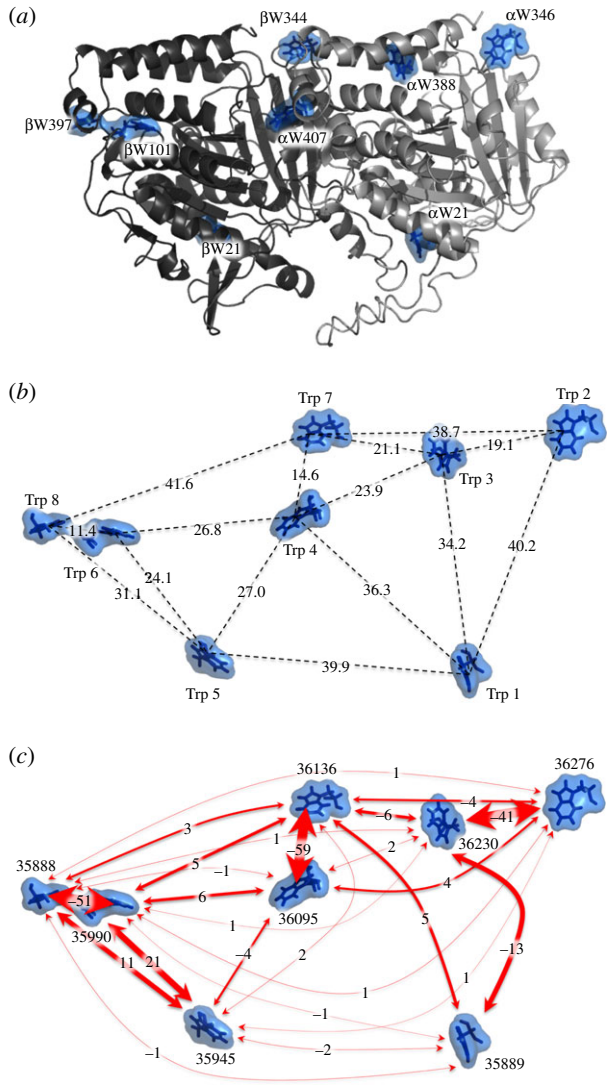

Figure 1. Arrangement of eight Trp chromophores in one tubulin αβ-dimer. Laterally oriented with the microtubule protofilament axis along the horizontal, microtubule surface above, microtubule lumen below. C-terminal tails not shown. (*a*) Location within tubulin dimer. (*b*) Spacings in angstrom. (*c*) Dipole couplings in cm^{-1} for a dielectric constant of 8.41. (Online version in colour.)

2. Results and discussion

The dominant spatial distribution and orientation of the Trp residues in tubulin after 8 ns of molecular dynamics simulation are shown in figure 1*a*. Between nearest-neighbours, spacing ranges between 11.4 and 41.6 Å (figure 1*b*). Importantly, this range is comparable to the distances between the bilin chromophores in cryptophyte marine algae, which has been shown to support quantum-coherent transfer of electronic excitation [11].

This spatial range, i.e. the average separation between neighbouring dipoles, is considered larger than the extension of the Trp transition densities and, so the point-dipole (PD) approximation was used to determine the inter-Trp excitonic couplings. In calculating the excitonic interaction coefficients, the choice of the dielectric constant value, and the method chosen for screening and local field effects is no trivial matter [28]. Typically, effective protein dielectric constant values are chosen between 2 and 4; however, experimental measures of the dielectric coefficients in protein hydrophobic pockets indicate this value is well above this range, arguing against this practice [29]. The experimentally measured tubulin optical dielectric value of 8.41 falls well outside this range [30], and is expected to have a significant impact on coupling strengths.

In the Förster approximation, accounting only for electrostatic screening effects owing to the polarizable medium being present between the dipoles, the dipolar couplings are small indicating little to no interaction between Trps, regardless of the dielectric value chosen. This is consistent with previous estimates of Förster dipole–dipole energy transfer between Trps in tubulin [19]. This study also calculates negligible intramolecular Trp–Trp energy transfer efficiencies in tubulin, however these are based on an estimated dielectric constant of 2 and an assumed spectral overlap integral for

Table 1. Site energies (diagonal, shown in italics are with respect to 35 888 cm^{-1}) and interaction energies in units of cm^{-1}.

Trp	1	2	3	4	5	6	7	8
1	*1*	0	−13	0	−2	−1	5	−1
2	0	*388*	−41	4	1	1	−4	1
3	−13	−41	*342*	2	0	1	−6	1
4	0	4	2	*207*	−4	6	−59	−1
5	−2	1	0	−4	*57*	21	2	11
6	−1	1	1	6	21	*102*	5	−51
7	5	−4	−6	−59	2	5	*248*	3
8	−1	1	1	−1	11	−51	3	*0*

Table 2. Excited state energies (cm^{-1}), and coefficients of the eigenvectors resulting from diagonalization of the Hamiltonian in table 1. Coefficients larger than 50% are shown in italics.

	contribution of Trp no.							
energies	1	2	3	4	5	6	7	8
35 863	0.04	0.00	0.00	−0.02	−0.22	0.40	−0.02	*0.89*
35 888	*−1.00*	0.00	−0.04	0.01	−0.05	0.01	0.02	0.02
35 946	−0.04	0.00	0.00	0.03	*0.95*	−0.12	0.00	0.28
36 014	0.01	0.00	0.00	0.12	−0.22	*−0.90*	0.09	0.35
36 054	0.02	0.00	0.01	*0.81*	0.01	0.15	*0.57*	−0.04
36 176	0.00	−0.14	−0.21	*0.56*	−0.02	0.00	*−0.79*	−0.01
36 208	0.04	−0.48	*−0.84*	−0.14	0.00	0.00	0.21	0.00
36 300	−0.02	*−0.86*	*0.50*	−0.01	0.00	0.00	0.00	0.00

N-acetyl-L-tryptophanamide in tris-(hydroxymethyl)aminomethane buffer at pH 7.8. As Trp is highly sensitive to its local environment [31], these results are seemingly inaccurate as the calculation does not accurately reflect the protein environment. However, accounting for electrostatic screening effects of the medium as well as local inhomogeneous field effects yields different results depending on the dielectric constant chosen. As the dielectric constant value increases between 2 and 8.41, the coupling strengths become increasingly non-negligible.

It must be noted here that using a dielectric constant value above 4 with the screening factor $f = \varepsilon_{opt}^{-1}[(\varepsilon_{opt} + 2)/3]^2$ yields $f > 1$. While this seems somewhat paradoxical in terms of a screening factor enhancing coupling, we consider it in the quantum viewpoint of Knox & van Amerongen [28] as the effect of the protein environment on the Trp dipole strengths. For the experimentally measured optical dielectric constant, coupling strengths up to 60 cm^{-1} are found with the most significant couplings being between Trps 2 and 3, Trps 4 and 7, and Trps 6 and 8. All coupling strengths for the dielectric constant of 8.41 are shown in figure 1*c* which accounts for the geometrical arrangement in place.

Calculated site energies using a dielectric constant value of 8.41 range between 35 888 and 36 276 cm^{-1}, giving the maximum energy difference between Trps of 388 cm^{-1}. These site energies are shown in figure 1*c* and table 1. Diagonalization of the Hamiltonian matrix (table 2) revealed that the degree of delocalization of excited state energies is relatively small. Only for the exciton states at 36 054, 36 176 and 36 300 cm^{-1} is there a significant delocalization over more than one pigment, with meaningful contributions between Trps 4 and 7, and Trps 2 and 3, owing to the close site energies between these pigments and their relatively large couplings.

While the coupling strengths become increasingly non-negligible as the dielectric constant value increases above 2, the general line shape of the simulated spectra does not align well with experiment for values between 2 and 4. This is most prominently seen in the circular dichroism (CD) spectra, and is not accounted for by simple shifts in E_0 alone (figure 2). However, when the experimentally measured optical dielectric value of tubulin is used the simulated spectra align well with experimental values (figure 2). This supports the use of the experimentally measured dielectric value over values between 2 and 4.

Population dynamics calculations from the Haken & Strobl [33] method were applied to the Hamiltonian in table 1 for initial excitations occurring on each of the eight Trp residues (figure 3). It was determined that coherent beatings last for approximately 600 fs with a pure dephasing rate of 50 cm^{-1}, when the excitation starts at Trps 2, 3, 4 or 7, and for less than 300 fs when starting at Trp 6 or 8. Excitations starting at Trp 1 or 5 did not produce any beating effects. When starting at Trp 2 or 3, the excitation can be seen to spread to Trp 4 and 7 reaching close to the equal population distribution of 0.125 within approximately 2 ps. Negligible exciton populations in the remaining Trps are observed in this time frame. When starting at Trp 4 or 7, the same effect is observed for Trps 2 and 3 with additional increases in exciton

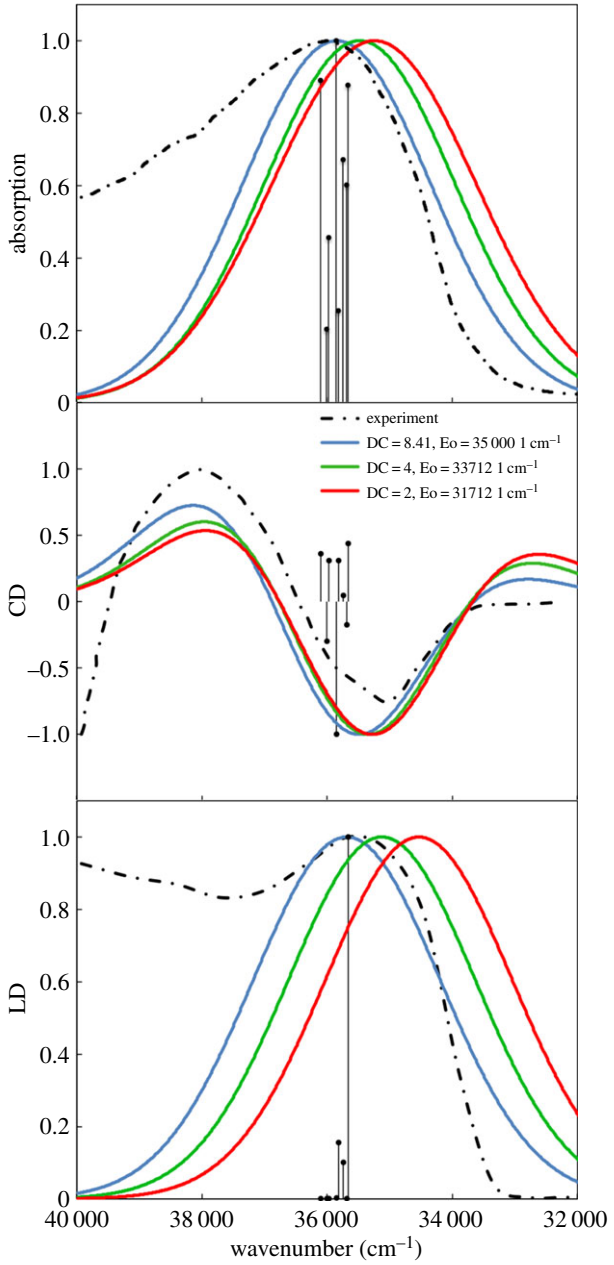

Figure 2. Alignment of calculated spectra with experiment. Experimental spectra, bare calculated stick spectra for DC 8.41, and calculated spectra with Gaussian broadening applied for the absorption, circular dichroism (CD) and linear dichroism (LD) of tubulin at 300 K. All values are plotted in arbitrary units similar to Vulto *et al.* [32]. (Online version in colour.)

population for Trps 5, 6 and 8 to approximately 0.06, spreading over the entire dimer. Owing to the Markovian assumption, the Haken–Strobl description of this system converges to an equal classical mixture of all sites in the long time limit, and most likely shows less coherence than other non-Markovian methods used in the study of LHCs [25,34]. Further analysis with non-Markovian methods may reveal longer-lived oscillations and more enhanced transfer dynamics.

Starting from the highest energy state the excitation travels from Trp $2 \rightarrow 3 \rightarrow 7 \rightarrow 4 \rightarrow 6 \rightarrow 8$ covering the length of the tubulin dimer. Stacking tubulin dimers end to end in a microtubule would most likely alter this energy landscape. However, as the interdimer spacing of Trps is uninterrupted (figure 4), it is feasible that such an arrangement could effectively transfer energy along the protofilament length via a combination of coherent tunnelling and incoherent relaxation/excitation. Additionally, the unique cylindrical lattice symmetries found in the tubulin lattices of microtubules may effectively serve to enhance transfer rates and distances, and potentially enable energy transfer along helical pathways. Generalized Förster effects [36], induced by geometrical symmetries, can enhance the exciton diffusion length along cylindrically symmetric structures [37], similar to the helical arrangement of tubulin, and its chromophores, in microtubules.

Is this effect unique to tubulin and microtubules? Trp is a ubiquitous amino acid found in almost all proteins in low abundance, and FRET between Trp residues and other fluorophores is a technique commonly used to probe protein structure and dynamics. In most cases, this RET is restricted to a single isolated protein, or between two adjacent interacting proteins or molecules. Crystalized globular proteins have the potential to efficiently transfer energy between Trp residues [38], yet these are rarely, if ever, found in biology. Protein polymers, such as the cell cytoskeleton, on the other hand, are pervasive in biology, offering candidate structures for this type of energy transmission. While crystal structures for the majority of cytoskeletal components do not currently exist, comparison of their amino acid sequences reveals that the majority of intermediate filaments have a Trp abundance less than a third of that found in tubulin (table 3) suggesting unfavourable conditions for RET. Only actin and synemin possess comparable densities, suggesting that polymers of these molecules could support RET similar to that in tubulin and microtubules. Although the crystal structure of actin is available and reveals 4 Trp per subunit with intramolecular separations ranging between 10 and 23 Å, the intermolecular distances between these Trp clusters is more than 40 Å (figure 4) suggesting unfavourable conditions for RET within a microfilament.

Whether coherent energy transfer in tubulin and microtubules has a biological role remains open. Such rapid signalling through Trp conduction pathways may coordinate the complex organization of the microtubule cytoskeleton required for the tasks of cell division, motor protein trafficking and motility. Microtubules have been shown to reorganize in a dose-dependent manner after exposure to UV light [39–42], with the greatest effect being observed around 280 nm [42]. Feasible mechanisms for these changes include the reduction of disulfide or peptide bonds induced by photoexcitation of Trp groups [43–46], or subtle protein structural changes owing to photo-induced alterations in Trp flexibility [46]. Such a signalling mechanism may explain the observed apparent UV mediated cell-to-cell influence on cell division [47]. Only further investigation, both theoretically and experimentally, will tell.

Thus, we conclude that, based on this initial analysis, the unique Trp network within an individual tubulin dimer can possess significant dipolar couplings capable of supporting quantum coherent beating effects similar to those observed in the FMO photosynthetic complex [4,5], LHCII [7,8], LH2 [9,10] and phycobiliprotein LHCs [11,12]. Furthermore, our results suggest that this network may support coherent energy transfer at physiological temperature between clusters of Trps in tubulin, and microtubule structures. One of the main objectives of this paper is to stimulate future experimental work in this area. While this is purely a computational prediction it supports the continued investigation of coherent energy transfer mechanisms in tubulin and microtubule lattices. Our predictions are experimentally feasible to verify employing the same methods as those used in the case of photosynthetic complexes.

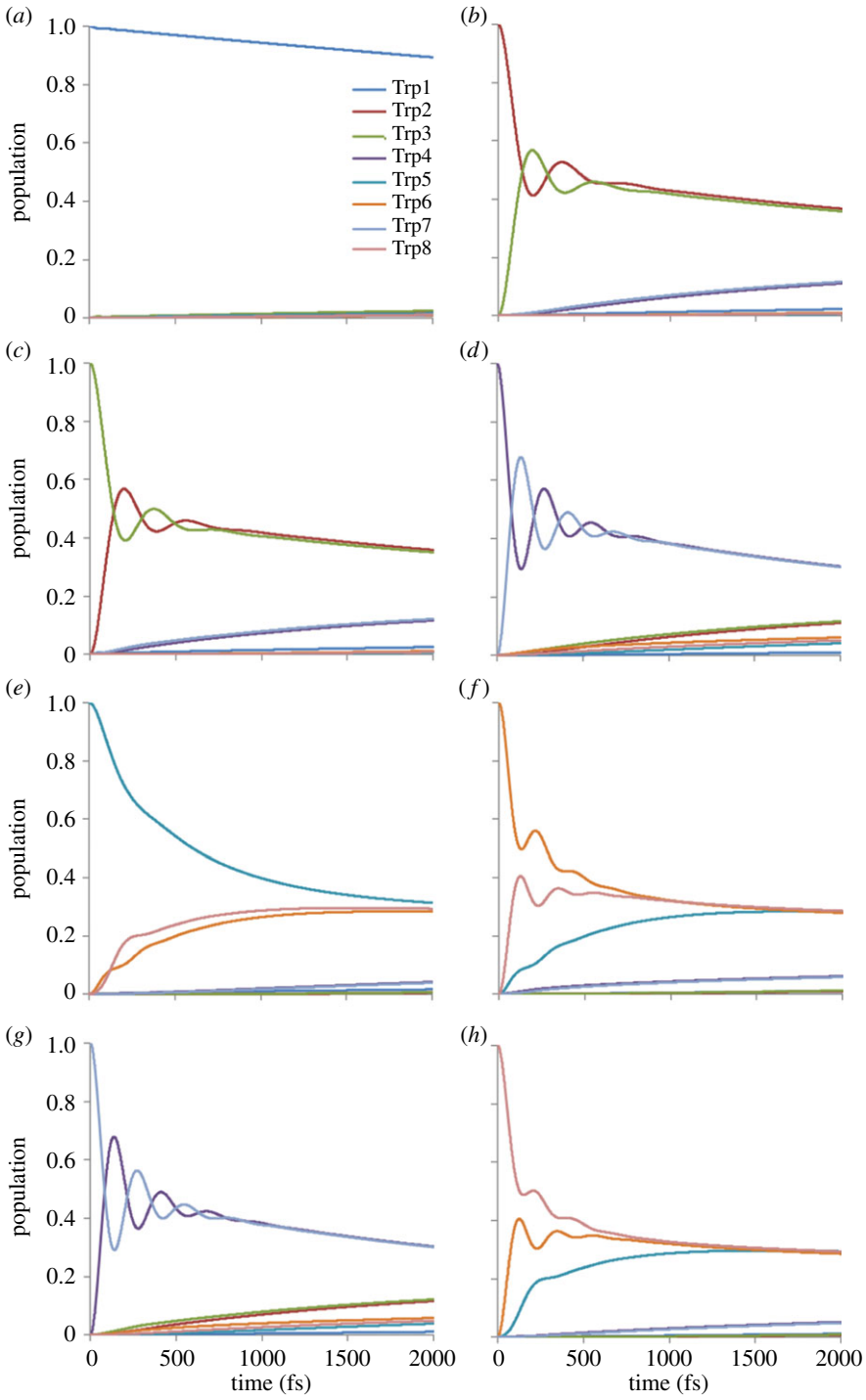

Figure 3. Time evolution of the exciton population of each tryptophan in tubulin via the Haken–Strobl model. Initial pure states are set as (*a*) Trp1: αW21, (*b*) Trp2: αW346, (*c*) Trp3: αW388, (*d*) Trp4: αW407, (*e*) Trp5: βW21, (*f*) Trp6: βW101, (*g*) Trp7: βW344 and (*h*) Trp8: βW397. (Online version in colour.)

3. Methods

Here, we give a brief summary of the computational procedures yielding site energies, excitonic couplings, optical spectra and time evolution of exciton populations. All data will be made available on request.

3.1. Molecular dynamics simulation/dominant tryptophan confirmation

MD simulations were performed based on previous methods [48,49], using NAMD [50]. Coordinates for the αβ-tubulin dimer at 3.5 Å, GDP, GTP and magnesium ion are from the Brookhaven National Laboratory Protein Data Bank [51] entry 1JFF [52] and PDB2PQR 1.7 [53] was used to generate per-atom charge and radius, at pH 7.0 using PROPKA [54,55], and the AMBER [56] force field. Swiss-PdbViewer v. 4.0 [57] was used to model the missing residues in the crystal structure (α-tubulin: 1, 35–60, 440–451, β-tubulin: 1, 438–455). GDP and GTP were modelled for use by the AMBER 94/99 force field by Meagher *et al.* [58]. PTRAJ, using the AMBER99SB force field [59] from AMBER 10 [56], was used to neutralize the system, add counterions to reproduce physiological ionic concentrations, and add a TIP3P water cube buffer of 25 Å (63 283 molecules of water). After minimization and heating to 310 K, equilibration occurred for 519 ps while gradually releasing constraints on backbone atoms. Then, using periodic boundary conditions, a 17 ns simulation occurred where atomic coordinates were saved from the trajectory every 2 ps.

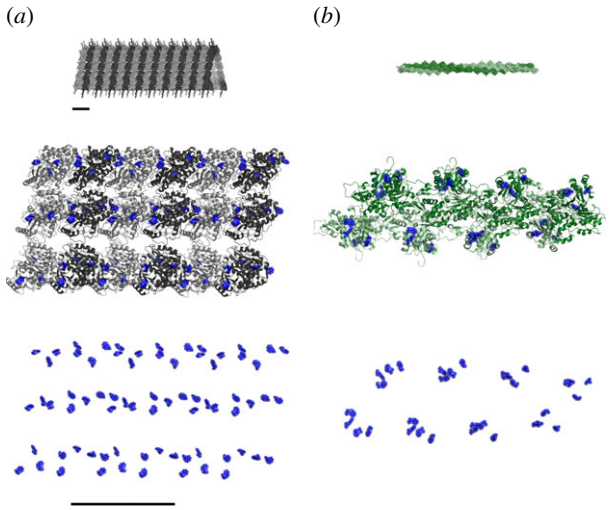

Figure 4. Tryptophan architectures in cytoskeletal filaments. (*a*) Tubulin based microtubule. (*b*) Actin-based microfilament. Scale bars are approximately 10 nm. Actin microfilaments are built using PDB ID: 2ZWH using the Oda *et al*. [35] filament model. (Online version in colour.)

PTRAJ was used to analyse the 17 ns trajectory for root mean square deviation (RMSD) of the backbone of non C-terminus residues of both alpha- and beta-tubulin, as well as the beta-factor of all residues. The RMSD was found to stabilize after approximately 8 ns. The final 8 ns of the total trajectory was chosen for further analysis. The GROMACS program g_cluster [60] was used to cluster the Trp atom positions of all frames via single linkage with a cut-off of 0.5 Å. The middle structure of the largest cluster was taken as the dominant conformation for the Trp residues.

3.2. Vertical excitation energies for tryptophan/site energy calculations

Site energies were derived from structure-based calculations of the free energy change of the protein–pigment complex (PPC) that occurs when the ground state charge density of Trp m is shifted to the first excited state, analogous to methods used for the FMO complex [26,61,62].

Quantum chemical calculations of the pigments *in vacuo* yield the charge distributions of the S_0 and $1L_a$ states and a contribution ΔE_{qm} to the $S_0 \rightarrow 1L_a$ transition energy owing to the differing orientations of the Trps. Trp side chains were each isolated from the dominant conformation (described above) and capped with a hydrogen atom to complete the valence. *Ab initio* geometry optimizations at the ground state were performed using density functional theory at the B3LYP/6-311G(d,p) [63] level. Quantum chemical calculations of the eight lowest singly excited vertical excitation energies of Trp were done using time-dependent density functional theory [64,65] at the B3LYP/6-311 + G(d,p) [63] level. All calculations were performed using ORCA v. 2.8 (http://cec.mpg.de/forum/).

The vertical transition energies for the $1L_a$ state of the Trp side chains were found to be comparable to previous work using similar methods [66], however, such as these results our values were found to be lower than experimentally determined values [66,67]. To align with experiment (38 473 cm^{-1}), a scaling factor of 1.02 was applied to the calculated values. The relative quantum correction, ΔE_{qm}, to the site energy was taken as the difference between the scaled and the experimental values.

The second part of the site energy calculation results in a contribution ΔE_{coul} owing to classical electrostatic interaction between the charge distributions of the S_0 and $1L_a$ states with the protein environment. Using the charge density coupling [61,62] method, the site energy shift of the mth Trp is calculated

Table 3. Tryptophan abundance in cytoskeletal constituent molecules.

cytoskeletal molecule	total residues	Trp residues	Trp abundance (%)
tubulin monomer	~450	4	0.9
actin	375	4	1.1
α-internexin	499	1	0.2
desmin	470	1	0.2
GFAP	432	1	0.2
keratin	564	2	0.3
neurofilament	916	3	0.3
peripherin	470	1	0.2
syncoilin	482	0	0.0
synemin	1565	15	1.0
vimentin	466	1	0.2

from the Coulomb interaction of the difference of the S_0 and $1L_a$ state partial charges $\Delta q_i{}^{(m)}$, obtained from the Löwdin atomic point charges in the above quantum chemical calculations, with the remaining background charges of the protein $q_j^{(\mathrm{bg})}$. As there can be large uncertainties when representing the Trp ring charge distribution as Löwdin atomic point charges, we have chosen to empirically scale the charges by a factor of 0.80 to improve alignment with the experimental spectra (described below). The electrochromic shift ΔE_{coul} is given as

$$\Delta E_{\mathrm{coul}} = \frac{1}{\varepsilon} \sum_{i=1}^{N} \sum_{j=1}^{K} \frac{\Delta q_i^{(m)} \cdot q_j^{(\mathrm{bg})}}{|r_i^{(m)} - r_j^{(\mathrm{bg})}|},$$

where N is the number of partial charges of the mth Trp side chain, K is the total number of background partial charges (including other Trp residues), and $|r_i^{(m)} - r_j^{(\mathrm{bg})}|$ is the distance between the ith difference partial charge of the mth pigment and the jth partial charge of the background. Background charges were taken from the AMBER99SB force field [59]. Here, we use the measured high-frequency dielectric for tubulin setting $\varepsilon = 8.41$ [30].

The site energy for the mth Trp is thus given as

$$E_m = E_0 + \Delta E_{\mathrm{qm}} + \Delta E_{\mathrm{coul}},$$

where E_0 is taken as 35 000 cm^{-1} (285 nm) to align with experimental spectra (described below).

3.3. Excitonic coupling interactions

Excitonic couplings are calculated using the PD approximation, valid as the distance between pigments is large compared with the extension of their transition densities. The PD excitonic coupling is given as

$$V_{mn} = f \frac{\mu_{\mathrm{vac}}^2}{R_{mn}^3} [\boldsymbol{e}_m \cdot \boldsymbol{e}_n - 3(\boldsymbol{e}_m \cdot \boldsymbol{e}_{mn})(\boldsymbol{e}_m \cdot \boldsymbol{e}_{mn})],$$

where $\boldsymbol{e}_m$ is a unit vector along the transition dipole moment of the mth Trp, the unit vector $\boldsymbol{e}_{mn}$ is oriented along the line connecting the centres of Trps m and n, μ_{vac} is the transition dipole moment of the $1L_a$ transition of Trp in vacuum, and the factor f effectively takes into account local field and screening effects in an effective way. In the simplest approximation, owing to Förster, $f = 1/\varepsilon_{\mathrm{opt}}$, accounting only for screening effects. However, when screening effects of the medium as well as local field effects are included, this becomes $f = \varepsilon_{\mathrm{opt}}^{-1}[(\varepsilon_{\mathrm{opt}} + 2)/3]^2$

[68–71]. Here, we consider both these cases. The optical dielectric constant for a typical protein environment is given in the range of 2–4; however, tubulin's high-frequency dielectric coefficient has been measured as 8.41 [30]. For comparison, we consider the two extremes of 2 and 8.41.

3.4. Alignment with experimental spectra

The tight-binding Hamiltonian for an interacting N-body system in the presence of a single excitation is given by [72]

$$H_S = \sum_{m=1}^{N} \varepsilon_m |m\rangle\langle m| + \sum_{m<n}^{N} V_{mn}(|m\rangle\langle n| + |n\rangle\langle m|),$$

where the states $|m\rangle$ denote the excitation being at site m. The site energies and coupling terms are given by ε_m and V_{mn}, respectively, and are calculated as described above. Exciton stick spectra for absorption, CD and linear dichroism (LD) were calculated from the orientations of the Trp molecules in the dominant confirmation and the diagonalized Hamiltonian matrix using the formula described by Pearlstein [73]. Experimental spectra were calculated by applying a Gaussian function to each exciton transition using an assumed full-width half maximum value of 3500 cm^{-1} as commonly observed for Trp [74,75]. These were then compared with experimental absorption, CD and LD spectra adapted from Mozo-Villarias *et al*. [76], Clark *et al*. [77] and Marrington *et al*. [78], respectively.

3.5. Exciton population dynamics

Time evolution of the exciton population in the Trp network in the presence of thermal fluctuations of the environment is modelled using the Haken & Strobl model [33]. Here, it is assumed that thermal fluctuations of the environment couple to the Trps by an electron–phonon interaction, acting only on the diagonal elements of the Hamiltonian system H_S, with the fluctuations being unbiased, uncorrelated and Gaussian in nature. Under these assumptions, the Haken–Strobl equation for the density operator ρ in the Schrödinger picture is given as

$$\dot{\rho}(t) = -\frac{i}{\hbar}[H_S, \rho(t)] + L_\phi(\rho(t)),$$

where the pure-dephasing Lindblad operator is given by

$$L_\phi(\rho(t)) = \sum_{m=1}^{n} \gamma_m \left[A_m \rho(t) A_m^\dagger - \frac{1}{2} A_m A_m^\dagger \rho(t) - \frac{1}{2} \rho(t) A_m A_m^\dagger \right],$$

with A_m and $A_m^\dagger$ being the creation and annihilation operators, and γ_m the pure dephasing rates for the mth Trp. As a reasonable assumption, here we take γ_m to be 50 cm^{-1} for all sites. All population dynamics were computed using QuTip 2 [79].

Acknowledgements. Thanks to Dr Chih-Yuan Tseng at Sinoveda Canada Inc., for his assistance in repairing the missing residues of the 1JFF crystal structure of the tubulin dimer, Dr J. Robert Johansson at the RIKEN, Advanced Science Institute for his help with the QuTip programming package and Dr David Sept at the University of Michigan for supplying files for the actin and microfilament structures.

Funding statement. Funding for this research was provided to J.A.T. by NSERC (Canada), to D.F. by CIHR (Canada), Alberta Innovates - Health Solutions, and the Alberta Cancer Foundation, and to T.J.A.C. by Nova Southeastern University's Center for Psychological Studies and Institute for Neuro-Immune Medicine. This research was conducted in collaboration with Dr Joel Zysman, Director of High Performance Computing, using the Pegasus platform at the University of Miami Center for Computational Science (CCS; http://ccs.miami.edu). This research was also enabled in part by support provided by WestGrid (www.westgrid.ca) and Compute Canada Calcul Canada (www.computecanada.ca).

References

1. Schrödinger E. 1944 *What is life? The physical aspect of the living cell*. Cambridge, UK: Cambridge University Press.
2. Lambert N, Chen YN, Cheng YC, Li CM, Chen GY, Nori F. 2012 Quantum biology. *Nat. Phys.* **9**, 10–18. (doi:10.1038/nphys2474)
3. Fleming GR, Scholes GD, Cheng YC. 2011 Quantum effects in biology. *Proc. Chem.* **3**, 38–57. (doi:10.1016/j.proche.2011.08.011)
4. Engel GS, Calhoun TR, Read EL, Ahn TK, Mančal T, Cheng YC, Blankenship RE, Fleming GR. 2007 Evidence for wavelike energy transfer through quantum coherence in photosynthetic systems. *Nature* **446**, 782–786. (doi:10.1038/nature05678)
5. Panitchayangkoon G, Hayes D, Fransted KA, Caram JR, Harel E, Wen J, Blankenship RE, Engel GS. 2010 Long-lived quantum coherence in photosynthetic complexes at physiological temperature. *Proc. Natl Acad. Sci. USA* **107**, 12 766–12 770. (doi:10.1073/pnas.1005484107)
6. Schlau-Cohen GS, Ishizaki A, Calhoun TR, Ginsberg NS, Ballottari M, Ballottari M, Bassi R, Fleming GR. 2012 Elucidation of the timescales and origins of quantum electronic coherence in LHCII. *Nat. Chem.* **4**, 389–395. (doi:10.1038/nchem.1303)
7. Calhoun TR, Ginsberg NS, Schlau-Cohen GS, Cheng YC, Ballottari M, Bassi R, Fleming GR. 2009 Quantum coherence enabled determination of the energy landscape in light-harvesting complex II. *J. Phys. Chem. B* **113**, 16 291–16 295. (doi:10.1021/jp908300c)
8. Schlau-Cohen GS, Calhoun TR, Ginsberg NS, Read EL, Ballottari M, Bassi R, van Grondelle R, Fleming GR. 2009 Pathways of energy flow in LHCII from two-dimensional electronic spectroscopy. *J. Phys. Chem. B* **113**, 15 352–15 363. (doi:10.1021/jp9066586)
9. Harel E, Engel GS. 2012 Quantum coherence spectroscopy reveals complex dynamics in bacterial light-harvesting complex 2 (LH2). *Proc. Natl Acad. Sci. USA* **109**, 706–711. (doi:10.1073/pnas.1110312109)
10. Ostroumov EE, Mulvaney RM, Cogdell RJ, Scholes GD. 2013 Broadband 2D electronic spectroscopy reveals a carotenoid dark state in purple bacteria. *Science* **340**, 52–56. (doi:10.1126/science.1230106)
11. Collini E, Wong CY, Wilk KE, Curmi PM, Brumer P, Scholes GD. 2010 Coherently wired light-harvesting in photosynthetic marine algae at ambient temperature. *Nature* **463**, 644–647. (doi:10.1038/nature08811)
12. Turner DB, Dinshaw R, Lee KK, Belsley M, Wilk KE, Curmi PMG, Scholes GD. 2012 Quantitative investigations of quantum coherence for a light-harvesting protein at conditions simulating photosynthesis. *Phys. Chem. Chem. Phys.* **14**, 4857–4874. (doi:10.1039/C2CP23670B)
13. Strümpfer J, Şener M, Schulten K. 2012 How quantum coherence assists photosynthetic light-harvesting. *J. Phys. Chem. Lett.* **3**, 536–542. (doi:10.1021/jz201459c)
14. Förster T. 1948 Excitation transfer. *Ann. Phys.* **2**, 12–19.
15. Andrews DL, Curutchet C, Scholes GD. 2011 Resonance energy transfer: beyond the limits. *Laser Photon. Rev.* **5**, 114–123. (doi:10.1002/lpor.201000004)
16. Beljonne D, Curutchet C, Scholes GD, Silbey RJ. 2009 Beyond Förster resonance energy transfer in biological and nanoscale systems. *J. Phys. Chem. B* **113**, 6583–6599. (doi:10.1021/jp900708f)
17. Würthner F, Kaiser TE, Saha-Möller CR. 2011 J-Aggregates: from serendipitous discovery to supramolecular engineering of functional dye materials. *Angew. Chem. Int. Ed.* **50**, 3376–3410. (doi:10.1002/anie.201002307)
18. Saikin SK, Eisfeld A, Valleau S, Aspuru-Guzik A. 2013 Photonics meets excitonics: natural and artificial molecular aggregates. *Nanophotonics* **2**, 21–38. (doi:10.1515/nanoph-2012-0025)
19. Sardar PS, Maity SS, Das L, Ghosh S. 2007 Luminescence studies of perturbation of tryptophan residues of tubulin in the complexes of tubulin with colchicine and colchicine analogues. *Biochemistry* **46**, 14 544–14 556. (doi:10.1021/bi701412k)

20. Monshouwer R, Abrahamsson M, van Mourik F, van Grondelle R. 1997 Superradiance and exciton delocalization in bacterial photosynthetic light-harvesting systems. *J. Phys. Chem. B* **101**, 7241–7248. (doi:10.1021/jp963377t)
21. Guha S, Rawat SS, Chattopadhyay A, Bhattacharyya B. 1996 Tubulin conformation and dynamics: a red edge excitation shift study. *Biochemistry* **35**, 13 426–13 433. (doi:10.1021/bi961251g)
22. Weber G, Shinitzky M. 1970 Failure of energy transfer between identical aromatic molecules on excitation at the long wave edge of the absorption spectrum. *Proc. Natl Acad. Sci. USA* **65**, 823–830. (doi:10.1073/pnas.65.4.823)
23. Hameroff S, Nip A, Porter M, Tuszynski J. 2002 Conduction pathways in microtubules, biological quantum computation, and consciousness. *Biosystems* **64**, 149–168. (doi:10.1016/S0303-2647(01)00183-6)
24. Hayes D, Griffin BG, Engel GS. 2013 Engineering coherence among excited states in synthetic heterodimer systems. *Science* **340**, 1431–1434. (doi:10.1126/science.1233828)
25. Shim S, Rebentrost P, Valleau S, Aspuru-Guzik A. 2012 Atomistic study of the long-lived quantum coherences in the Fenna–Matthews–Olson complex. *Biophys. J.* **102**, 649–660. (doi:10.1016/j.bpj.2011.12.021)
26. Müh F, Madjet MEA, Adolphs J, Abdurahman A, Rabenstein B, Ishikita H, Knapp EW, Renger T. 2007 α-Helices direct excitation energy flow in the Fenna–Matthews–Olson protein. *Proc. Natl Acad. Sci. USA* **104**, 16 862–16 867. (doi:10.1073/pnas.0708222104)
27. Huh J, Saikin SK, Brookes JC, Valleau S, Fujita T, Aspuru-Guzik A. 2014 Atomistic study of energy funneling in the light-harvesting complex of green sulfur bacteria. *J. Am. Chem. Soc.* **136**, 2048–2057. (doi:10.1021/ja412035q)
28. Knox RS, van Amerongen H. 2002 Refractive index dependence of the Förster resonance excitation transfer rate. *J. Phys. Chem. B* **106**, 5289–5293. (doi:10.1021/jp013927+)
29. García-Moreno BE, Dwyer JJ, Gittis AG, Lattman EE, Spencer DS, Stites WE. 1997 Experimental measurement of the effective dielectric in the hydrophobic core of a protein. *Biophys. Chem.* **64**, 211–224. (doi:10.1016/S0301-4622(96) 02238-7)
30. Mershin A, Kolomenski AA, Schuessler HA, Nanopoulos DV. 2004 Tubulin dipole moment, dielectric constant and quantum behavior: computer simulations, experimental results and suggestions. *Biosystems* **77**, 73–85. (doi:10.1016/j.biosystems.2004.04.003)
31. Pan CP, Muiño PL, Barkley MD, Callis PR. 2011 Correlation of tryptophan fluorescence spectral shifts and lifetimes arising directly from heterogeneous environment. *J. Phys. Chem. B* **115**, 3245–3253. (doi:10.1021/jp111925w)
32. Vulto SI, de Baat MA, Louwe RJ, Permentier HP, Neef T, Miller M, van Amerongen H, Aartsma TJ. 1998 Exciton simulations of optical spectra of the FMO complex from the green sulfur bacterium *Chlorobium tepidum* at 6 K. *J. Phys. Chem. B* **102**, 9577–9582. (doi:10.1021/jp982095l)
33. Haken H, Strobl G. 1973 An exactly solvable model for coherent and incoherent exciton motion. *Z Phys* **262**, 135–148. (doi:10.1007/BF01399723)
34. Rebentrost P, Chakraborty R, Aspuru-Guzik A. 2009 Non-Markovian quantum jumps in excitonic energy transfer. *J. Chem. Phys.* **131**, 184102. (doi:10.1063/1.3259838)
35. Oda T, Iwasa M, Aihara T, Maéda Y, Narita A. 2009 The nature of the globular- to fibrous-actin transition. *Nature* **457**, 441–445. (doi:10.1038/nature07685)
36. Scholes GD, Jordanides XJ, Fleming GR. 2001 Adapting the Förster theory of energy transfer for modeling dynamics in aggregated molecular assemblies. *J. Phys. Chem. B* **105**, 1640–1651. (doi:10.1021/jp003571m)
37. Abasto DF, Mohseni M, Lloyd S, Zanardi P. 2012 Exciton diffusion length in complex quantum systems: the effects of disorder and environmental fluctuations on symmetry-enhanced supertransfer. *Phil. Trans. R. Soc. A* **370**, 3750–3770. (doi:10.1098/rsta.2011.0213)
38. Desie G, Boens N, De Schryver FC. 1986 Study of the time-resolved tryptophan fluorescence of crystalline alpha-chymotrypsin. *Biochemistry* **25**, 8301–8308. (doi:10.1021/bi00373a026)
39. Krasylenko Y, Yemets A, Blume Y. 2013 Plant microtubules reorganization under the indirect UV-B exposure and during UV-B-induced programmed cell death. *Plant Signal. Behav.* **8**, e24031. (doi:10.4161/psb.24031)
40. Staxén I, Bergounioux C, Bornman JF. 1993 Effect of ultraviolet radiation on cell division and microtubule organization in *Petunia hybrida* protoplasts. *Protoplasma* **173**, 70–76. (doi:10.1007/BF01378863)
41. Zamansky GB, Chou IN. 1987 Environmental wavelengths of ultraviolet light induce cytoskeletal damage. *J. Invest. Dermatol.* **89**, 603–606. (doi:10.1111/1523-1747.ep12461366)
42. Zaremba TG, LeBon TR, Millar DB, Smejkal RM, Hawley RJ. 1984 Effects of ultraviolet light on the *in vitro* assembly of microtubules. Biochem*istry* **23**, 1073–1080. (doi:10.1021/bi00301a006)
43. Neves-Petersen MT, Gryczynski Z, Lakowicz J, Fojan P, Pedersen S, Petersen E, Bjørn Petersen S. 2002 High probability of disrupting a disulphide bridge mediated by an endogenous excited tryptophan residue. *Protein Sci.* **11**, 588–600. (doi:10.1110/ps.06002)
44. Vanhooren A, Devreese B, Vanhee K, Van Beeumen J, Hanssens I. 2002 Photoexcitation of tryptophan groups induces reduction of two disulfide bonds in goat α-lactalbumin. Biochem*istry* **41**, 11 035–11 043. (doi:10.1021/bi0258851)
45. Wu LZ, Sheng YB, Xie JB, Wang W. 2008 Photoexcitation of tryptophan groups induced reduction of disulfide bonds in hen egg white lysozyme. *J. Mol. Struct.* **882**, 101–106. (doi:10.1016/j.molstruc.2007.09.016)
46. Weisenborn P, Meder H, Egmond MR, Visser TJ, van Hoek A. 1996 Photophysics of the single tryptophan residue in *Fusarium solani* cutinase: evidence for the occurrence of conformational substates with unusual fluorescence behaviour. *Biophys. Chem.* **58**, 281–288. (doi:10.1016/0301-4622(95)00079-8)
47. Fels D. 2009 Cellular communication through light. *PLoS ONE* **4**, e5086. (doi:10.1371/journal.pone.0005086)
48. Barakat K, Mane J, Friesen D, Tuszynski J. 2010 Ensemble-based virtual screening reveals dual-inhibitors for the p53-MDM2/MDMX interactions. *J. Mol. Graph. Model.* **28**, 555–568. (doi:10.1016/j.jmgm.2009.12.003)
49. Friesen DE, Barakat KH, Semenchenko V, Perez-Pineiro R, Fenske BW, Mane J, Wishart DS, Tuszynski JA. 2012 Discovery of small molecule inhibitors that interact with γ-tubulin. *Chem. Biol. Drug Des.* **79**, 639–652. (doi:10.1111/j.1747-0285.2012.01340.x)
50. Phillips JC *et al*. 2005 Scalable molecular dynamics with NAMD. *J. Comput. Chem.* **26**, 1781–1802. (doi:10.1002/jcc.20289)
51. Bernstein FC, Koetzle TF, Williams GJ, Meyer Jr EF, Brice MD, Rodgers JR, Kennard O, Shimanouchi T, Tasumi M. 1977 The protein data bank: a computer-based archival file for macromolecular structures. *J. Mol. Biol.* **112**, 535–542. (doi:10.1016/0003-9861(78)90204-7)
52. Löwe J, Li H, Downing KH, Nogales E. 2001 Refined structure of $\alpha\beta$-tubulin at 3.5 Å resolution. *J. Mol. Biol.* **313**, 1045–1057. (doi:10.1006/jmbi.2001.5077)
53. Dolinsky TJ, Nielsen JE, McCammon JA, Baker NA. 2004 PDB2PQR: an automated pipeline for the setup of Poisson–Boltzmann electrostatics calculations. *Nucleic Acids Res.* **32**, W665–W667. (doi:10.1093/nar/gkh381)
54. Li H, Robertson AD, Jensen JH. 2005 Very fast empirical prediction and rationalization of protein pKa values. *Proteins: Struct. Funct. Bioinf.* **61**, 704–721. (doi:10.1002/prot.20660)
55. Bas DC, Rogers DM, Jensen JH. 2008 Very fast prediction and rationalization of pKa values for protein–ligand complexes. *Proteins: Struct. Funct. Bioinf.* **73**, 765–783. (doi:10.1002/prot.22102)
56. Case DA *et al*. 2008 *Amber 10*. San Francisco, CA: University of California Press.
57. Guex N, Peitsch MC. 1997 SWISS-MODEL and the Swiss-PdbViewer: an environment for comparative protein modeling. *Electrophoresis* **18**, 2714–2723. (doi:10.1002/elps.1150181505)
58. Meagher KL, Redman LT, Carlson HA. 2003 Development of polyphosphate parameters for use with the AMBER force field. *J. Comput. Chem.* **24**, 1016–1025. (doi:10.1002/jcc.10262)
59. Hornak V, Abel R, Okur A, Strockbine B, Roitberg A, Simmerling C. 2006 Comparison of multiple Amber force fields and development of improved protein backbone parameters. *Proteins: Struct. Funct. Bioinf.* **65**, 712–725. (doi:10.1002/prot.21123)
60. Van Der Spoel D, Lindahl E, Hess B, Groenhof G, Mark AE, Berendsen HJ. 2005 GROMACS: fast, flexible, and free. *J. Comput. Chem.* **26**, 1701–1718. (doi:10.1002/jcc.20291)
61. Adolphs J, Müh F, Madjet MEA, Renger T. 2008 Calculation of pigment transition energies in the

FMO protein. *Photosynth. Res.* **95**, 197–209. (doi:10.1007/s11120-007-9248-z)

62. Adolphs J, Müh F, Madjet MEA, Busch MSA, Renger T. 2010 Structure-based calculations of optical spectra of photosystem I suggest an asymmetric light-harvesting process. *J. Am. Chem. Soc.* **132**, 3331–3343. (doi:10.1021/ja9072222)
63. Krishnan RBJS, Binkley JS, Seeger R, Pople JA. 1980 Self-consistent molecular orbital methods. XX. A basis set for correlated wave functions. *J. Chem. Phys.* **72**, 650. (doi:10.1063/1.438955)
64. Koch W, Holthausen MC. 2001 *A chemist's guide to density functional theory,* vol. 2. Weinheim, Germany: Wiley-VCH.
65. Parr RG, Yang W. 1989 *Density functional theory of atoms and molecules*. New York, NY: Oxford University Press.
66. Rogers DM, Besley NA, O'Shea P, Hirst JD. 2005 Modeling the absorption spectrum of tryptophan in proteins. *J. Phys. Chem. B* **109**, 23 061–23 069. (doi:10.1021/jp053309j)
67. Serrano-Andrés L, Roos BO. 1996 Theoretical study of the absorption and emission spectra of indole in the gas phase and in a solvent. *J. Am. Chem. Soc.* **118**, 185–195. (doi:10.1021/ja952035i)
68. Juzeliūnas G, Andrews DL. 1994 Quantum electrodynamics of resonant energy transfer in condensed matter. *Phys. Rev. B* **49**, 8751. (doi:10.1103/PhysRevB.49.8751)
69. Juzeliūnas G, Andrews DL. 1994 Quantum electrodynamics of resonant energy transfer in condensed matter. II. Dynamical aspects. *Phys. Rev. B* **50**, 13371. (doi:10.1103/PhysRevB.50.13371)
70. Mennucci B, Curutchet C. 2011 The role of the environment in electronic energy transfer: a molecular modeling perspective. *Phys. Chem. Chem. Phys.* **13**, 11 538–11 550. (doi:10.1039/C1CP20601J)
71. Scholes GD, Fleming GR. 2000 On the mechanism of light harvesting in photosynthetic purple bacteria: B800 to B850 energy transfer. *J. Phys. Chem. B* **104**, 1854–1868. (doi:10.1021/jp993435l)
72. May V, Kühn O. 2004 *Charge and energy transfer dynamics in molecular systems, 2nd, Revised and Enlarged Edition*. Weinheim, Germany: Wiley-VCH.
73. Pearlstein RM. 1991 Theoretical interpretation of antenna spectra. In *Chlorophylls* (ed. H Scheer), pp. 1047–1978. Boca Raton, FL: CRC press.
74. Léonard J, Portuondo-Campa E, Cannizzo A, van Mourik F, van der Zwan G, Tittor J, Haacke S, Chergui M. 2009 Functional electric field changes in photoactivated proteins revealed by ultrafast Stark spectroscopy of the Trp residues. *Proc. Natl Acad. Sci. USA* **106**, 7718–7723. (doi:10.1073/pnas.0812877106)
75. Schenkl S, van Mourik F, van der Zwan G, Haacke S, Chergui M. 2005 Probing the ultrafast charge translocation of photoexcited retinal in bacteriorhodopsin. *Science* **309**, 917–920. (doi:10.1126/science.1111482)
76. Mozo-Villarias A, Morros A, Andreu JM. 1991 Thermal transitions in the structure of tubulin. *Eur. Biophys. J.* **19**, 295–300. (doi:10.1007/BF00183318)
77. Clark DC, Martin SR, Bayley PM. 1981 Conformation and assembly characteristics of tubulin and microtubule protein from bovine brain. *Biochemistry* **20**, 1924–1931. (doi:10.1021/bi00510a031)
78. Marrington R, Seymour M, Rodger A. 2006 A new method for fibrous protein analysis illustrated by application to tubulin microtubule polymerisation and depolymerisation. *Chirality* **18**, 680–690. (doi:10.1002/chir.20305)
79. Johansson JR, Nation PD, Nori F. 2013 QuTiP 2: a Python framework for the dynamics of open quantum systems. *Comp. Phys. Comm.* **184**, 1234. (doi:10.1016/j.cpc.2012.11.019)